nature medicine

Brief Communication

https://doi.org/10.1038/s41591-024-03453-1

Bioaccumulation of microplastics in decedent human brains

Received: 29 April 2024

Accepted: 9 December 2024

Published online: 03 February 2025

Check for updates

Alexander J. Nihart[1,12], Marcus A. Garcia[1,12], Eliane El Hayek[1,12], Rui Liu[1], Marian Olewine[1], Josiah D. Kingston[1], Eliseo F. Castillo[2], Rama R. Gullapalli[3], Tamara Howard[4], Barry Bleske[5], Justin Scott[6], Jorge Gonzalez-Estrella[6], Jessica M. Gross[7], Michael Spilde[8], Natalie L. Adolphi[9], Daniel F. Gallego[9], Heather S. Jarrell[9], Gabrielle Dvorscak[9], Maria E. Zuluaga-Ruiz[10], Andrew B. West[11] & Matthew J. Campen[1]

Rising global concentrations of environmental microplastics and nanoplastics (MNPs) drive concerns for human exposure and health outcomes. Complementary methods for the robust detection of tissue MNPs, including pyrolysis gas chromatography–mass spectrometry, attenuated total reflectance–Fourier transform infrared spectroscopy and electron microscopy with energy-dispersive spectroscopy, confirm the presence of MNPs in human kidney, liver and brain. MNPs in these organs primarily consist of polyethylene, with lesser but significant concentrations of other polymers. Brain tissues harbor higher proportions of polyethylene compared to the composition of the plastics in liver or kidney, and electron microscopy verified the nature of the isolated brain MNPs, which present largely as nanoscale shard-like fragments. Plastic concentrations in these decedent tissues were not influenced by age, sex, race/ethnicity or cause of death; the time of death (2016 versus 2024) was a significant factor, with increasing MNP concentrations over time in both liver and brain samples ($P = 0.01$). Finally, even greater accumulation of MNPs was observed in a cohort of decedent brains with documented dementia diagnosis, with notable deposition in cerebrovascular walls and immune cells. These results highlight a critical need to better understand the routes of exposure, uptake and clearance pathways and potential health consequences of plastics in human tissues, particularly in the brain.

Environmental concentrations of anthropogenic microplastic and nanoplastic (MNP), polymer-based particulates ranging from 500 µm in diameter down to 1 nm, have increased exponentially over the past half century[1,2]. The extent to which MNPs cause human harm or toxicity is unclear, although recent studies associated MNP presence in carotid atheromas with increased inflammation and risk of future adverse cardiovascular events[3,4]. In controlled cell culture and animal exposure studies, MNPs exacerbate disease or drive toxic outcomes, but at concentrations with unclear relevance to human exposures and body burdens[5,6]. The mantra of the field of toxicology—'dose makes the poison' (Paracelsus)—renders such discoveries as easily anticipated; what is not clearly understood is the tissue distribution and internal dose of MNPs in humans, which confounds our ability to interpret the controlled exposure study results.

So far, visual microscopic spectroscopy methods have identified particulates in organs, such as the lungs, intestine[7] and placenta[8]. These methods are often limited to larger (>5 µm) particulates; thus, smaller nanoplastics are unintentionally excluded. As a new approach,

A full list of affiliations appears at the end of the paper. e-mail: mcampen@salud.unm.edu

https://doi.org/10.1038/s41591-024-03453-1

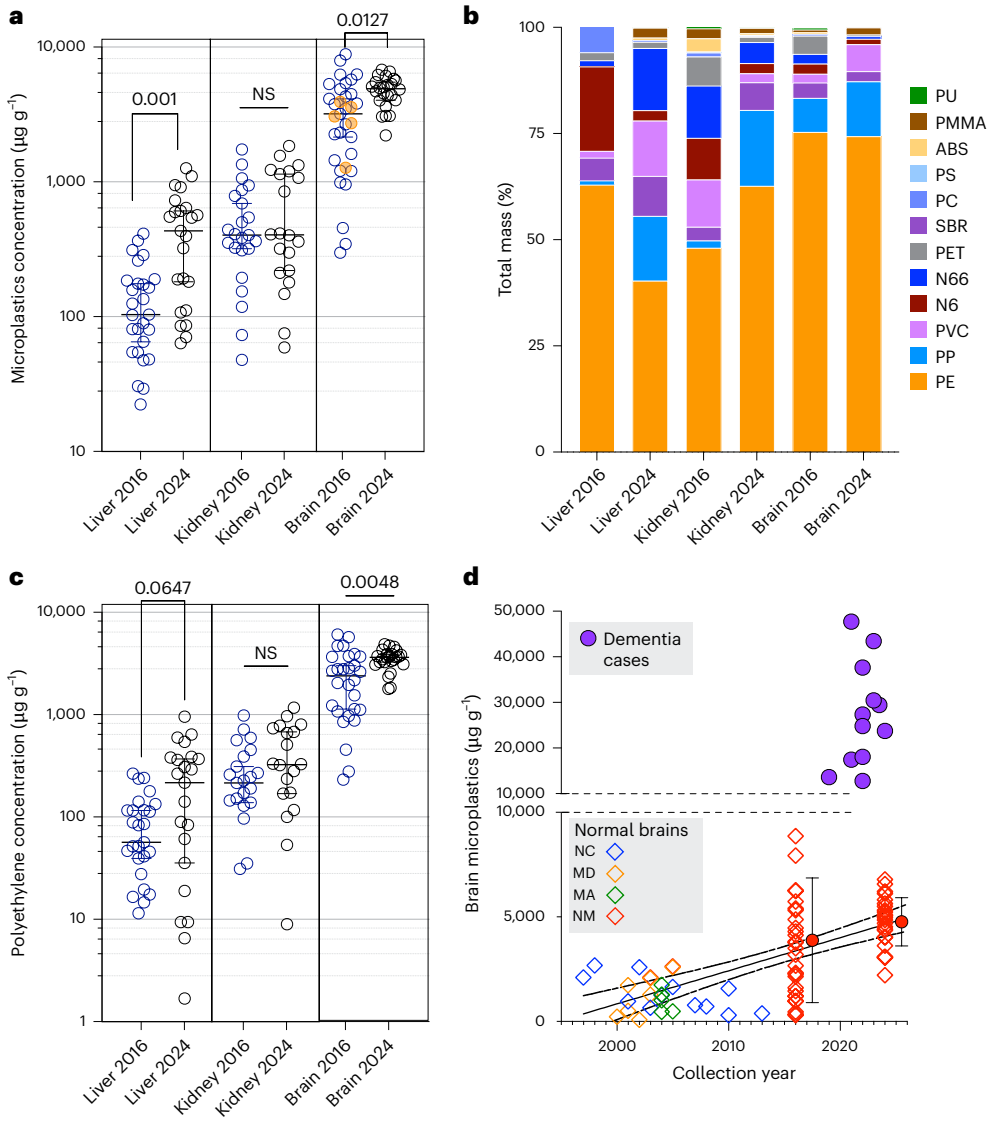

Fig. 1 | Overview of total MNP concentrations from all decedent samples from liver, kidney and brain. a, Microplastic concentrations in liver, kidney and brain decedent human samples ($n = 20–28$ separate participants for each timepoint; Supplementary Table 1) from the UNM OMI. Data are shown on a $\log_{10}$ scale, with the bar representing the group median value and 95% confidence interval. Orange-colored symbols in the 2016 brain samples were analyzed independently at Oklahoma State University. *P* values from Mann–Whitney tests (two-sided) indicate significant differences in samples from the same organ between 2016 and 2024 (with more comprehensive statistical treatments in Supplementary Methods—Statistical analysis). Brain MNP concentrations were significantly higher than liver and kidney, analyzed by two-way ANOVA ($P < 0.0001$). **b**, Overall distribution of 12 different polymers suggests a greater accumulation of PE in the brain relative to liver or kidney (average shown per group; see Extended Data Fig. 1 for individual data). **c**, PE (which was in the highest abundance and consistently had the highest confidence spectra) concentrations in all organs followed similar trends compared to total plastics (also represented as group median value and 95% confidence interval; two-sided Mann–Whitney test). **d**, Additional brain samples from specimens collected from 1997 to 2013 were obtained from the Duke Kathleen Price Bryan Brain Bank in North Carolina ($n = 13$, blue diamonds; NC), the Harvard Brain Tissue Resource Center in Massachusetts ($n = 9$, green diamonds; MA) and the National Institute of Child Health and Human Development Brain and Tissue Bank at the University of Maryland ($n = 5$, orange diamonds; MD) show lower concentrations of microplastics. Brain samples from decedents with diagnosed dementia ($n = 12$, purple circles) from UNM exhibit far greater MNP concentrations than brain tissues from participants without dementia from New Mexico (red thin-outline diamonds; NM). Overall linear regression trend was significantly nonzero ($P < 0.0001$) with an $R^2 = 0.3982$; summary points for 2016 and 2024 normal UNM OMI brains reflect mean ± s.d. N66, nylon 66; ABS, acrylonitrile butadiene styrene; PET, polyethylene terephthalate; N6, nylon-6; PMMA, poly(methyl methacrylate); PU, polyurethane; PC, polycarbonate; PS, polystyrene.

pyrolysis gas chromatography–mass spectrometry (Py-GC/MS) has been applied to blood[9], placentas[10] and recently major blood vessels[3,4] in a manner that appears more cumulative, quantitative and less biased when coupled with orthogonal methods. Py-GC/MS data between labs has been comparable, providing confidence in this method for human tissue analysis[3,9,10]. Here we applied Py-GC/MS in concert with visualization methods to assess the relative distribution of MNPs in major organ systems from human decedent livers, kidneys and brains.

Results and discussion

We obtained de-identified, postmortem human liver (right central parenchyma), kidney (wedge piece containing cortex and medulla) and brain (frontal cortex) samples, retrospectively from 2016 and 2024 autopsy specimens (Supplementary Table 1), in cooperation with and approval from the University of New Mexico (UNM) Office of the Medical Investigator (OMI) in Albuquerque, New Mexico (NM), under the guidance of a trained forensic pathologist (D.F.G.) who selected consistent regions

from all organs. Py-GC/MS measurements of MNP concentrations in decedent liver and kidney specimens were similar, with the median value of total plastics at 433 and 404 μg g^{-1}, respectively, from 2024 samples (Fig. 1a and Supplementary Table 1). These were higher than previously published data for human placentas (median = 63.4 μg g^{-1})[10] and testes (median = 299 μg g^{-1})[11]. Brain samples, all derived from the frontal cortex, exhibited substantially higher concentrations of MNPs than liver or kidney (two-way analysis of variance (ANOVA), $P < 0.0001$), but comparable to recently published Py-GC/MS data from carotid plaques[4], with a median of 3345 μg g^{-1} (25–75%: 1,267–5,213 μg g^{-1}) in 2016 samples and 4917 μg g^{-1} (25–75%: 4,026–5,608 μg g^{-1}) in 2024 samples (Fig. 1a and Supplementary Table 1).

Liver and brain samples from 2024 had significantly higher concentrations of MNPs than 2016 samples on both post hoc multiple comparisons of the two-way ANOVA (Supplementary Tables 4–7 and Supplementary Fig. 6), consistent with results from a multiple regression analysis of brain concentrations considering the potential influence of other demographic variables (Supplementary Tables 8–10). Five brain samples from 2016 (highlighted in orange in Fig. 1a) were analyzed independently by colleagues at Oklahoma State University using Py-GC/MS, and those values were consistent with our findings ($P = 0.49$ for a Student's t test comparing UNM and OSU data). The proportion of polyethylene (PE) in the brain (75% on average) was greater relative to other polymers and compared to PE in the liver and kidney ($P < 0.0001$; Fig. 1b and Extended Data Fig. 1). PE, polypropylene (PP), polyvinyl chloride (PVC) and styrene-butadiene rubber (SBR) concentrations specifically increased from 2016 to 2024 in liver and brain samples (Fig. 1c and Extended Data Fig. 2). PE predominance was confirmed with attenuated total reflectance–Fourier transform infrared spectroscopic analysis from five brain samples, although other polymers were not as consistent in prevalence, possibly due to differences in prevalence across size distributions and limited sampling (Supplementary Tables 9–13 and Supplementary Figs. 17–25).

To expand these findings, we obtained brain tissue from earlier time frames (1997–2013) with a mean age of death comparable to the NM cohorts (52.8 ± 34.3 years) from locations in the eastern United States, along with samples from a repository of dementia cases at UNM. Py-GC/MS analysis revealed lower overall MNP concentrations in East Coast samples (median = 1,254 μg g^{-1}; Supplementary Table 1 and Fig. 1d). While geographical differences cannot be ruled out, we applied a simple linear regression including all normal brain biospecimen data, which revealed significantly increasing trends for total plastics, PE, PP, PVC and SBR (Extended Data Fig. 2). To extend findings to a specific neurological condition, Py-GC/MS was conducted on 12 dementia cases collected in the NM OMI. These cases included Alzheimer's disease ($n = 6$), vascular dementia ($n = 3$) and other dementia ($n = 3$) specimens from 2019 to 2024. Py-GC/MS analysis revealed total plastics concentrations in dementia samples (median = 26,076 μg g^{-1}; Fig. 1d and Supplementary Table 1) that were higher than in any normal frontal cortex cohort ($P < 0.0001$ by two-sided t test). Atrophy of brain tissue, impaired blood–brain barrier integrity and poor clearance mechanisms are hallmarks of dementia and would be anticipated to increase MNP concentrations; thus, no causality is assumed from these findings.

Using scanning electron microscopy (SEM) and polarization wave microscopy, refractory inclusions were identified in all organs histologically (Fig. 2, Extended Data Fig. 3 and Supplementary Figs. 7–16). Within the liver, these inclusions were widely dispersed but also notably aggregated within acellular regions consistent with the expected frequency and morphology of lipid droplets, with rod-shaped particles in the 1–5 μm size range (Extended Data Fig. 3a). In the kidney, an elevated presence of refractile inclusions of similar sizes was noted in glomeruli and along tubules (Extended Data Fig. 3a–d). Based on elevated concentrations of polymers identified by Py-GC/MS in these tissues, we suspected that much of the MNPs may be present in the nanoscale range, too small for visualization by light microscopy. Transmission electron microscopy (TEM) was therefore conducted on the dispersed KOH-insoluble pellets obtained from the liver and kidney (Extended Data Fig. 3e,f and Supplementary Fig. 9). While this visualization method cannot provide spectroscopic confirmation of polymer composition, we observed common shapes and sizes across samples and tissue types. Particulates isolated from the pellets and well-dispersed appeared shard-like and were typically less than 0.4 μm in length, consistent with recent findings of nanoplastics in farmed mussels[12]. SEM with energy-dispersive spectroscopy confirmed that particles observed in livers, kidneys and brains were principally composed of carbon (Extended Data Figs. 4–7). Based on the larger morphology of particulates observed in situ versus those isolated and dispersed from the pellets of digested tissue, we postulate that aggregation of nanoplastics may occur in the liver and kidney.

In brain tissues, larger (1–5 μm) refractile inclusions were not seen, but smaller particulates (<1 μm) were noted in the brain parenchyma (Fig. 2a–c and Supplementary Figs. 10–15). Given the resolution limitations of light microscopy, we examined resuspended brain pellets by TEM, which revealed largely 100–200 nm long shards or flakes (Fig. 2d and Supplementary Figs. 9 and 16). In situ, we confirmed that particles found in the brain were carbon-based by SEM with energy-dispersive X-ray spectrometry (EDS; Extended Data Figs. 6 and 7). In dementia samples, many refractile inclusions were prominent in regions with inflammatory cells and along the vascular wall (Fig. 2e,f). MNP uptake and distribution pathways are poorly understood, and the mechanism of how nanoplastics are delivered to and taken up into the brain is unknown. Insights from *Daphnia magna* suggest clathrin-dependent endocytosis and macropinocytosis may underlie nanoplastic translocation within the intestine[13]; we posit a similar uptake may occur in human ingestion of lipids that would also facilitate selective transfer into the brain. While blood was not cleared from the decedent's organs during autopsy, it is unlikely that the nanoplastics in the brain are selectively contained in the vascular compartment, as the kidneys and livers would also have comparable blood volumes.

While we suspected that MNPs might accumulate in the body over a lifespan, the lack of correlation between total plastics and decedent age ($P = 0.87$ for brain data) does not support this (Supplementary Fig. 1). However, total mass concentration of plastics in the brains analyzed in this study increased by approximately 50% in the past 8 years. Thus, we postulate that the exponentially increasing environmental concentrations of MNPs[2,14] may analogously increase internal maximal concentrations. Although there are few studies to draw on yet performed in mammals, in zebrafish exposed to constant concentrations, nanoplastic uptake increased to a stable plateau and cleared after exposure[15]; however, the maximal internal concentrations were increased proportionately with higher nanoplastic exposure concentrations. While clearance rates and elimination routes of MNPs from the brain remain uncharacterized, it is possible that an equilibrium—albeit variable between people—might occur between exposure, uptake and clearance, with environmental exposure concentrations ultimately determining the internal body burden.

Although the current data derive from multiple tissue banks and two analytic sites replicating key results, the new analytical Py-GC/MS methods applied here are yet to be widely adopted and refined into standardized tests for clinical specimens. Both analytical laboratories (UNM and OSU) observed a ~25% within-sample coefficient of variation, which does not alter the conclusions regarding temporal trends or accumulation in brains relative to other tissues, given the magnitude of those effects. Numerous quality control steps ensure that external contaminants are not impacting the results, including Py-GC/MS assessment of KOH and formalin storage control sample 'blanks' and measurements of the polymer composition of all plastic tubes and pipette tips that are essential in the digestion and measurement process (Supplementary Figs. 2–4). Decedent specimen collections over the past 30 years were not focused on minimizing external plastic

https://doi.org/10.1038/s41591-024-03453-1

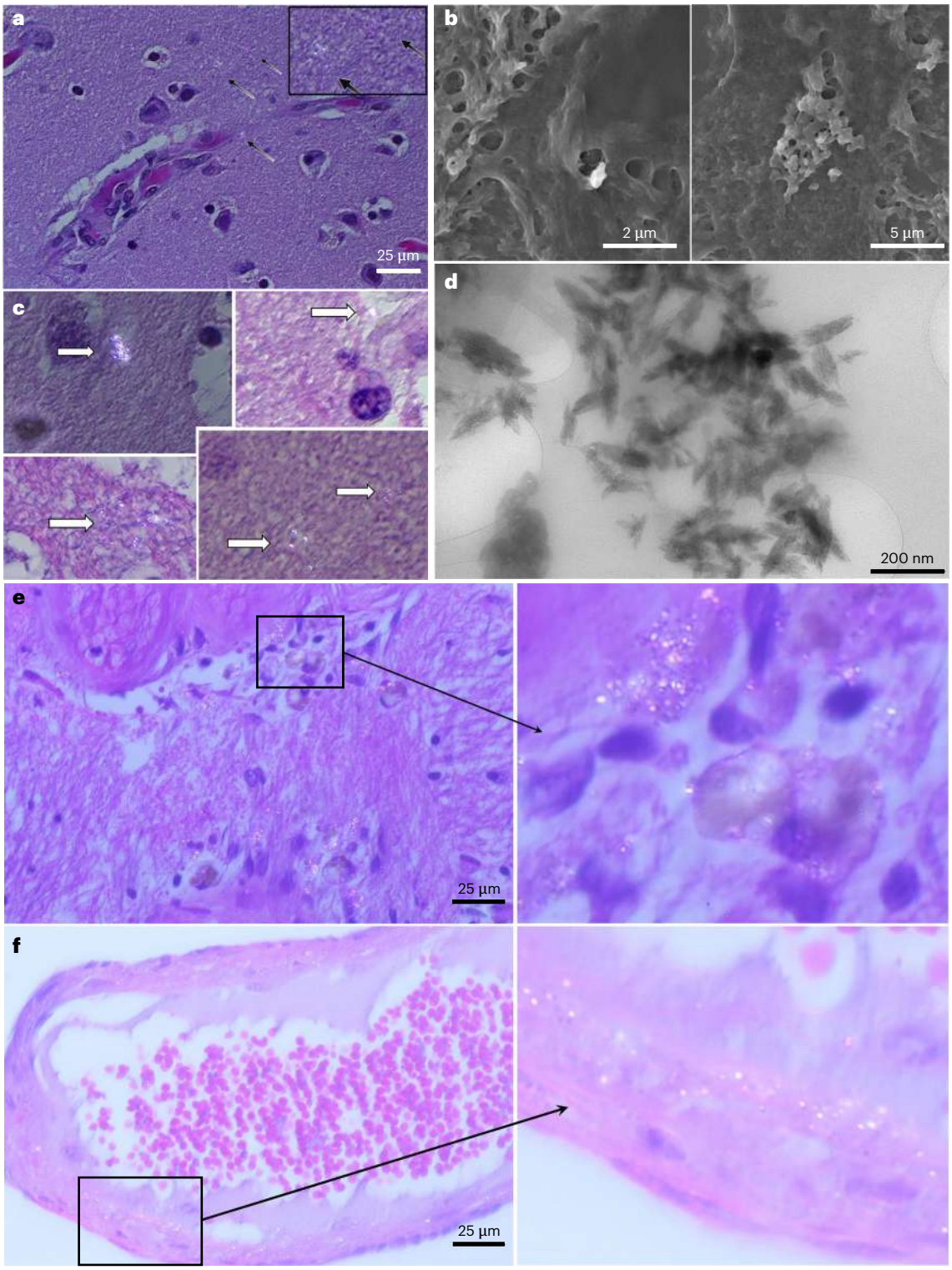

Fig. 2 | Visualization of putative plastics in the brain. a,**b**, Polarization wave microscopy (**a**, black arrows indicate refractory inclusions; inset is a digital magnification for clarity) and SEM (**b**, visual fields are 15.4 and 20.1 µm wide) were used to scan sections of brain from decedent human samples. **c**, Large (>1 µm) inclusions were not observed; additional polarization wave examples are highlighted (white arrows highlight submicron refractory inclusions). Resolution limitations of these technologies drove the use of TEM to examine the extracts from the pellets used for Py-GC/MS. **d**, Example TEM images resolved innumerable shard- or flake-like solid particulates following dispersion, with dimensions largely <200 nm in length and <40 nm in width. **e**,**f**, Polarization wave microscopy reveals substantially more refractile inclusions in dementia cases, especially in regions with associated immune cell accumulation (**e**) and along the vascular walls (**f**). All images were collected on a small subset of participants ($n = 10$ for normal brains; $n = 3$ for dementia cases) to provide visual evidence to support analytical chemistry.

contamination. However, given the consistent nature of handling and processing across all organ samples within objectively clean clinical and forensic settings, the significant accumulation of MNPs in the brain cannot be dismissed as an artifact of contamination. Furthermore, the 2016 samples were stored for 84–96 months compared to only 2–4 months for the 2024 samples, which exhibited greater concentrations of polymer. Thus, contamination from plastic storage vessels should not influence the conclusions. For the brain, especially, greater attention to anatomical features, such as white versus gray matter, vascularization and glia content, should be carefully evaluated in future studies to reduce variation. Finally, by obtaining only a single sample from each organ for each participant, distribution heterogeneity within tissues remains uncharacterized.

Our estimates of polymer mass concentration could be impacted by several factors that may lead to overestimation or underestimation. The KOH digestion extensively eliminated biological material from the pellets through saponification of triglycerides and denaturing of proteins (Supplementary Fig. 5). However, the final pellets still contained unknown residual biomatrix, which could present challenges for mass spectral interference. KOH reduced the liver and kidney mass by 99.4%, while the brain samples were reduced by 91.8%, that is, the resultant average pellet mass derived from 500 mg of starting material was approximately 3 mg and 41 mg, respectively. This discrepancy is proportional to, and consistent with, the mass of the polymer measured. However, unknown organic molecules likely remain and influence the resultant Py-GC/MS spectra. Lipids have been noted as a potential source of interference in Py-GC/MS analysis of PE[16]. Our method of KOH digestion and physical separation of solids was designed to reduce this concern, rather than augment it with a liquid–liquid extraction in organic solvents that would selectively drive lipid partitioning. Furthermore, the spectra suggest a reduction of longer carbon chains in the pyrolysis chromatogram, which is potentially due to advanced oxidative degradation of the MNPs and excess carbonyl formation that may lead to an underestimation of the concentration, as our standards are created with pristine polymers[17,18]. Finally, given the observed small size of nanoscale particles isolated from the human specimens (typically <200 nm in length), it is likely that ultracentrifugation incompletely collected nanoplastics in the analytical samples, also contributing to potential underestimation. The shape and size of observed nanoparticles in the isolated material from human specimens taxes the limits of modern analytical instrumentation but may reflect an end-stage product of plastic degradation that is uniquely suited for human uptake and accumulation.

Conclusions

The present data suggest a trend of increasing MNP concentrations in the brain and liver. The majority of MNPs found in tissues consist of PE and appear to be nanoplastic shards or flakes. MNP concentrations in normal decedent brain samples were 7–30 times greater than the concentrations seen in livers or kidneys, and brain samples from dementia cases exhibited even greater MNP presence. These data are associative and do not establish a causal role for such particles affecting health. For this, refinements to the analytical techniques, more complex study designs and much larger cohorts are needed. Given the exponentially rising environmental presence of MNPs[19–21], these data compel a much larger effort to understand whether MNPs have a role in neurological disorders or other human health effects.

Online content

Any methods, additional references, Nature Portfolio reporting summaries, source data, extended data, supplementary information, acknowledgements, peer review information; details of author contributions and competing interests; and statements of data and code availability are available at https://doi.org/10.1038/s41591-024-03453-1.

References

1. Thompson, R. C. et al. Lost at sea: where is all the plastic? *Science* **304**, 838 (2004).
2. Stubbins, A., Law, K. L., Munoz, S. E., Bianchi, T. S. & Zhu, L. Plastics in the Earth system. *Science* **373**, 51–55 (2021).
3. Liu, S. et al. Microplastics in three types of human arteries detected by pyrolysis-gas chromatography/mass spectrometry (Py-GC/MS). *J. Hazard. Mater.* **469**, 133855 (2024).
4. Marfella, R. et al. Microplastics and nanoplastics in atheromas and cardiovascular events. *N. Engl. J. Med.* **390**, 900–910 (2024).
5. Dong, C. D. et al. Polystyrene microplastic particles: in vitro pulmonary toxicity assessment. *J. Hazard. Mater.* **385**, 121575 (2020).
6. Dibbon, K. C. et al. Polystyrene micro- and nanoplastics cause placental dysfunction in mice. *Biol. Reprod.* **110**, 211–218 (2023).
7. Zhu, L. et al. Tissue accumulation of microplastics and potential health risks in human. *Sci. Total Environ.* **915**, 170004 (2024).
8. Ragusa, A. et al. Plasticenta: first evidence of microplastics in human placenta. *Environ. Int.* **146**, 106274 (2021).
9. Leslie, H. A. et al. Discovery and quantification of plastic particle pollution in human blood. *Environ. Int.* **163**, 107199 (2022).
10. Garcia, M. A. et al. Quantitation and identification of microplastics accumulation in human placental specimens using pyrolysis gas chromatography mass spectrometry. *Toxicol. Sci.* **199**, 81–88 (2024).
11. Hu, C. et al. Microplastic presence in dog and human testis and its potential association with sperm count. *Toxicol. Sci.* **200**, 235–240 (2024).
12. Fraissinet, S., De Benedetto, G. E., Malitesta, C., Holzinger, R. & Materić, D. Microplastics and nanoplastics size distribution in farmed mussel tissues. *Commun. Earth Environ.* **5**, 128 (2024).
13. Das, A., Terry, L. R., Sanders, S., Yang, L. & Guo, H. Confocal surface-enhanced raman imaging of the intestinal barrier crossing behavior of model nanoplastics in *Daphnia magna*. *Environ. Sci. Technol.* **58**, 11615–11624 (2024).
14. Landrigan, P. J. Plastics, fossil carbon, and the heart. *N. Engl. J. Med.* **390**, 948–950 (2024).
15. Habumugisha, T., Zhang, Z., Fang, C., Yan, C. & Zhang, X. Uptake, bioaccumulation, biodistribution and depuration of polystyrene nanoplastics in zebrafish (*Danio rerio*). *Sci. Total Environ.* **893**, 164840 (2023).
16. Rauert, C., Pan, Y., Okoffo, E. D., O'Brien, J. W. & Thomas, K. V. Extraction and pyrolysis-GC-MS analysis of polyethylene in samples with medium to high lipid content. *J. Environ. Expo. Assess.* **1**, 13 (2022).
17. Ainali, N. M., Bikiaris, D. N. & Lambropoulou, D. A. Aging effects on low- and high-density polyethylene, polypropylene and polystyrene under UV irradiation: an insight into decomposition mechanism by Py-GC/MS for microplastic analysis. *J. Anal. Appl. Pyrol.* **158**, 105207 (2021).
18. Toapanta, T. et al. Influence of surface oxidation on the quantification of polypropylene microplastics by pyrolysis gas chromatography mass spectrometry. *Sci. Total Environ.* **796**, 148835 (2021).
19. Wang, C. H., Zhao, J. & Xing, B. S. Environmental source, fate, and toxicity of microplastics. *J. Hazard. Mater.* **407**, 124357 (2021).
20. Geyer, R., Jambeck, J. R. & Law, K. L. Production, use, and fate of all plastics ever made. *Sci. Adv.* **3**, e1700782 (2017).
21. Landrigan, P. J. et al. The Minderoo-Monaco Commission on plastics and human health. *Ann. Glob. Health* **89**, 23 (2023).

[1]Department of Pharmaceutical Sciences, College of Pharmacy, University of New Mexico Health Sciences, Albuquerque, NM, USA. [2]Division of Gastroenterology and Hepatology, Department of Internal Medicine, University of New Mexico Health Sciences Center, Albuquerque, NM, USA. [3]Department of Pathology, University of New Mexico Health Sciences Center, Albuquerque, NM, USA. [4]Department of Cell Biology and Physiology, School of Medicine, University of New Mexico Health Sciences Center, Albuquerque, NM, USA. [5]Department of Pharmacy Practice and Administrative Sciences, College of Pharmacy, University of New Mexico Health Sciences Center, Albuquerque, NM, USA. [6]School of Civil & Environmental Engineering, Oklahoma State University, Stillwater, OK, USA. [7]Clinical and Translational Science Center, University of New Mexico Health Sciences Center, Albuquerque, NM, USA. [8]Department of Earth and Planetary Sciences, University of New Mexico, Albuquerque, NM, USA. [9]Office of the Medical Investigator, University of New Mexico, Albuquerque, NM, USA. [10]Grupo de Investigación en Rehabilitación de la Universidad del Valle (GIRUV), Cali, Colombia. [11]Duke Center for Neurodegeneration and Neurotherapeutics, Duke University, Durham, NC, USA. [12]These authors contributed equally: Alexander J. Nihart, Marcus A. Garcia, Eliane El Hayek. ✉e-mail: mcampen@salud.unm.edu

Methods

Human tissue samples

The same tissue collection protocol at the UNM OMI was used for 2016 and 2024. Small pieces of representative organs (3–5 cm^3) were routinely collected at autopsy and stored in 10% formalin. Additionally, decedent samples from a cohort with confirmed dementia ($n = 12$) were included, also collected at the UNM OMI under identical procedures. Limited demographic data (age, sex, race/ethnicity, cause of death and date of death) were available due to the conditions of specimen approval; age of death, race/ethnicity and sex were relatively consistent across cohorts (Supplementary Table 1). Additional brain samples ($n = 28$) were obtained from repositories on the East Coast of the United States to provide a greater range for the year of death (going back to 1997). All studies were approved by the respective Institutional Review Boards.

Py-GC/MS detection of polymer solids

Py-GC/MS is an informative and reliable method to determine plastic concentrations in liquid and solid tissue samples, with ample assurance of accuracy, quality and rigor[3,4,9,10]. Briefly, solid particulates are isolated from chemically digested tissue samples and then combusted to reveal signature mass spectra for select polymers (see full details in Supplementary Methods—Pyrolysis gas chromatography–mass spectrometry (PY-GC/MS)). Thus, the Py-GC/MS output is derived from enriched solid polymer particles and not soluble components from the digested tissue. Samples (~500 mg) were digested with 10% potassium hydroxide for at least 3 days at 40 °C. Samples were then ultracentrifuged at 100,000*g* for 4 h to generate a pellet enriched in solid materials resistant to such digestion, which included polymer-based solids[10]. A 1–2 mg portion of the resulting pellet was then analyzed by single-shot Py-GC/MS and compared to a microplastics-$CaCO_3$ standard containing the following 12 specific polymers: PE, PVC, nylon 66, SBR, acrylonitrile butadiene styrene, polyethylene terephthalate, nylon-6, poly(methyl methacrylate), polyurethane, polycarbonate, PP and polystyrene. Py-GCMS operating settings and polymer pyrolyzate targets are described in Supplementary Tables 2 and 3, with examples of spectra from samples, standards and blanks shown in Supplementary Figs. 2–4. Polymer spectra were identified via F-Search MPs v2.1 software (Frontier Labs). The resulting data were normalized to the original sample weight to render a mass concentration (μg g^{-1}).

Data analysis

Details of statistical analyses (normalization steps, two-way ANOVA and multiple regression) are provided in the Supplementary Methods—Statistical analysis.

Reporting summary

Further information on research design is available in the Nature Portfolio Reporting Summary linked to this article.

Data availability

More extensive methods and results are provided in the online Supplementary Information. Full demographic and analytical results are provided in Dryad (https://doi.org/10.5061/dryad.b8gtht7p8).

Acknowledgements

We thank J.D. Hesch at Hesch Consulting for her critical review of this manuscript. This research was funded by the National Institute of Health (P20 GM130422 (to M.J.C. and R.G.), R01 ES032037 (to E.F.C.), R01 ES014639 (to M.J.C.), K12 GM088021 (to M.A.G.), P50 MD015706 (to E.E.H. and J.G.-E.), P30 ES032755 (to B.B.), UL1 TR001449 (to J.G.) and R15 ES034901 (to J.S. and J.G.-E.)).

Author contributions

M.J.C., E.F.C., M.A.G., E.E.H., B.B. and J.G.-E. conceptualized the project and secured funding. M.J.C., A.J.N., M.A.G., J.S., J.G.-E., E.E.H., R.R.G., D.F.G., J.M.G., B.B. and A.B.W. wrote the original draft of the paper. D.F.G., A.J.N., M.O., H.S.J., G.D., M.E.Z.-R., N.L.A. and A.B.W. did sample procurement, identification and diagnosis. M.A.G., R.L., J.D.K., J.G.-E. and J.S. performed analytical chemistry and sample analysis. H.S.J., M.J.C., E.F.C. and A.B.W. provided compliance assurance. E.E.H., T.H., M.S. and R.R.G. performed imaging. J.M.G. and M.J.C. performed statistical analysis.

Competing interests

The authors declare no competing interests.

Additional information

Extended data is available for this paper at https://doi.org/10.1038/s41591-024-03453-1.

Supplementary information The online version contains supplementary material available at https://doi.org/10.1038/s41591-024-03453-1.

Correspondence and requests for materials should be addressed to Matthew J. Campen.

Peer review information *Nature Medicine* thanks Gary Miller and the other, anonymous, reviewer(s) for their contribution to the peer review of this work. Primary Handling Editor: Jerome Staal, in collaboration with the *Nature Medicine* team.

https://doi.org/10.1038/s41591-024-03453-1

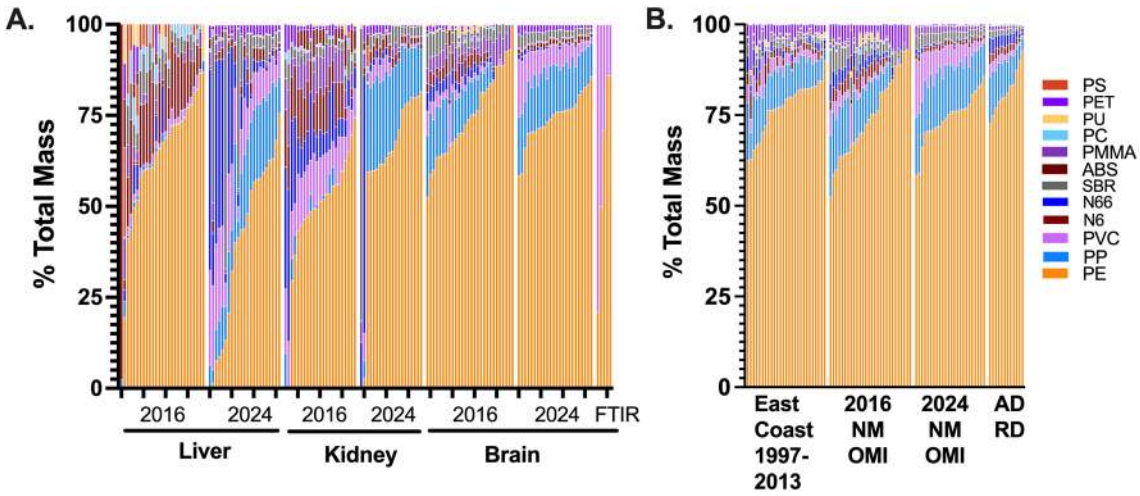

Extended Data Fig. 1 | Overall compositional outcomes, in relative proportion of the total polymer mass. Overall compositional outcomes, in relative proportion of the total mass, are shown for (**a**) liver, kidney and brain samples and (**b**) a cross-comparison of data for brains from all cohorts (polyethylene (PE), polypropylene (PP), polystyrene (PS), acrylonitrile butadiene styrene resin (ABS), sytrene-butadiene rubber (SBR), polymethyl methacrylate (PMMA), polycarbonate (PC), polyvinyl chloride (PVC), polyurethane (PU), polyethylene terephthalate (PET), nylon-6 (N6) and nylon-6,6 (N66)). Additionally, relative proportions of polymers from Fourier transform infrared (FTIR) spectroscopic analysis in brains are shown for comparison (last 5 columns in **a**). In general, 4 polymers, PE, PP and PVC comprise approximately 90% of the mass of samples, with nylon being an additional major component in some samples. Each column represents a unique subject (see Supplementary Table 1 for demographic data).

https://doi.org/10.1038/s41591-024-03453-1

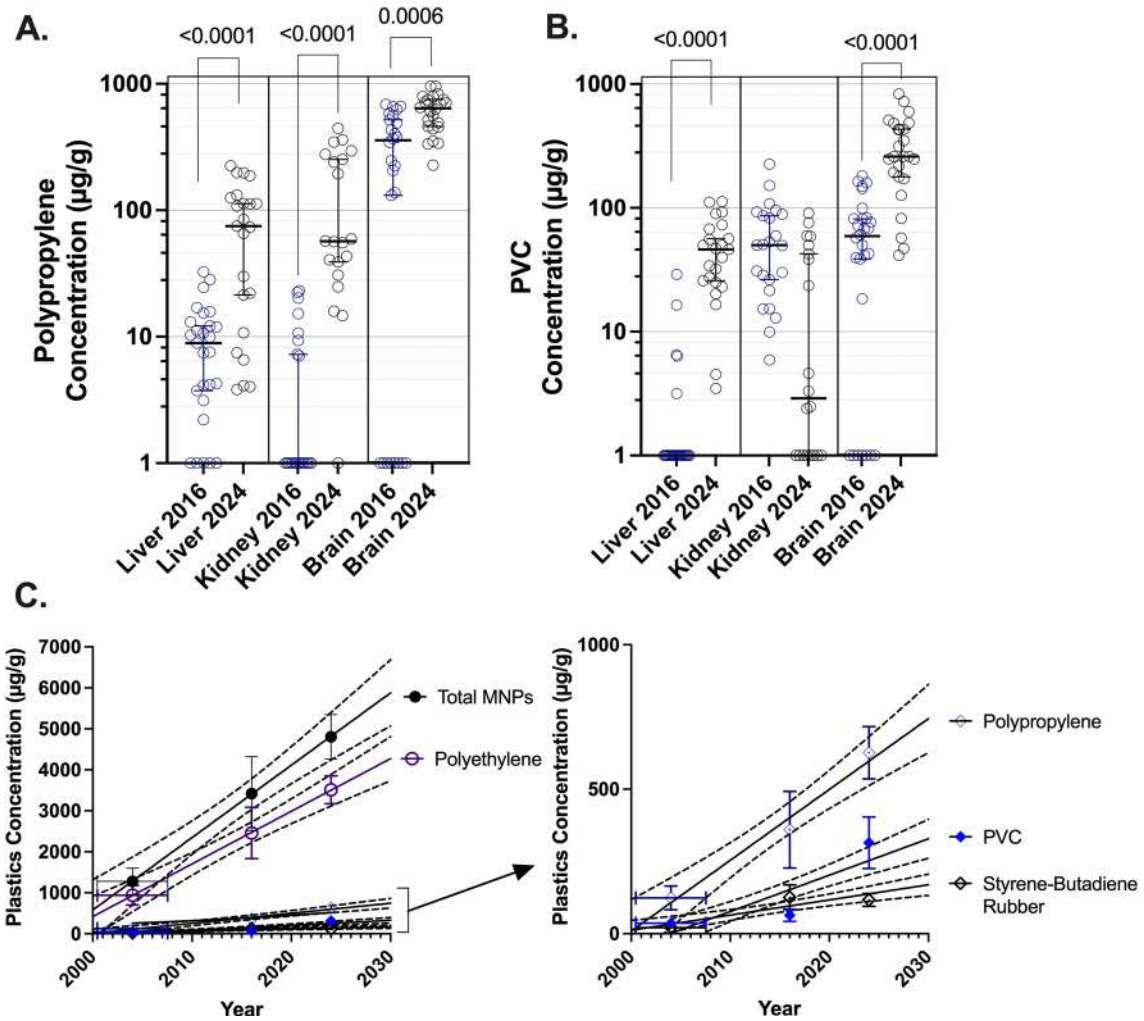

Extended Data Fig. 2 | Comparison of polypropylene and polyvinyl chloride in all organs across time. Comparison of (**a**) polypropylene and (**b**) polyvinyl chloride across time and organs for NM OMI samples (see subject demographics in Supplementary Table 1). P-values shown indicate significant differences between 2016 and 2024 samples by a two-sided Mann–Whitney test. **c**, Simple linear regression (shown with 95% CI represented by dashed lines) was performed for total plastics, polyethylene, polypropylene, polyvinyl chloride and styrene-butadiene rubber measured in normal decedent brains from 2004 (average of east coast samples), 2016 and 2024 (NM OMI samples). Mean ± 95% CI are shown for each cluster of samples. Regression analysis for all plastics rendered a p-value < 0.0001 for each polymer, with R^2 values ranging from 0.25 to 0.48.

https://doi.org/10.1038/s41591-024-03453-1

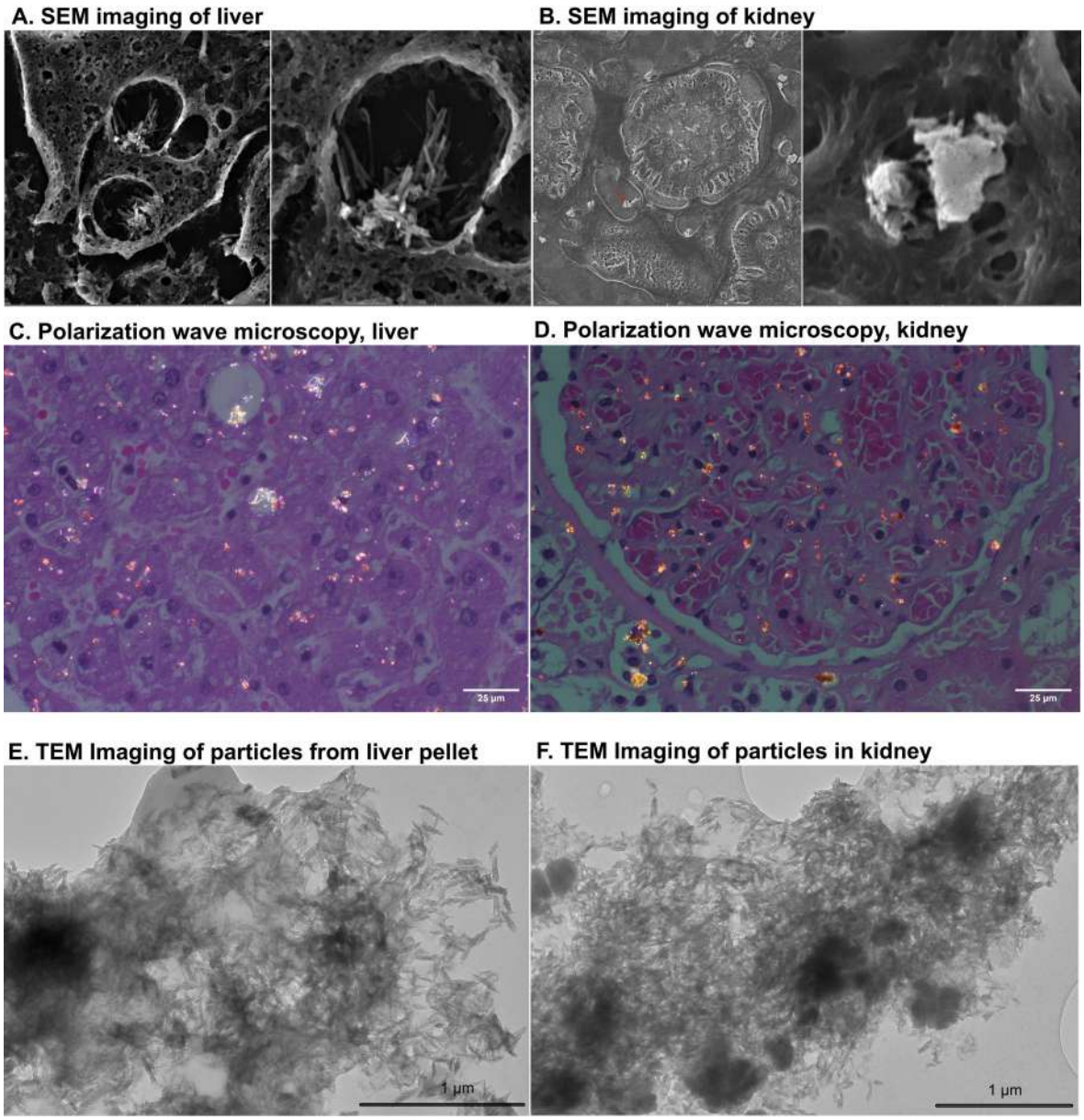

Extended Data Fig. 3 | TEM, polarization wave microscopy, and SEM images of putative microplastics from liver and kidney. Example SEM (**a**,**b**) and polarization wave microscopy (**c**,**d**) images of decedent histological specimens and TEM images (**e**,**f**) of nanoparticulates derived from liver (left) and kidney (right). While these methods do not permit spectroscopic identification of particulate molecular composition, the bulk of particulates that were predominantly polymer as assessed by ATR–FTIR appear to be of these sizes and shapes. Energy-dispersive spectroscopy confirmed that particles were carbon-based and not mineral (Extended Data Figs. 4 and 5). Visual fields for SEM were 39.5 µm and 15.4 µm (**a**) and 135 µm and 9 µm (**b**). Example TEM images from the dispersed pellet that was derived from KOH digestion and ultracentrifugation resolved innumerable shard-like solid particulates, with dimensions largely <200 nm in length and <40 nm in width. Polarization wave microscopic images were collected on a small subset of subjects (N = 12) to provide visual evidence to support analytical chemistry.

https://doi.org/10.1038/s41591-024-03453-1

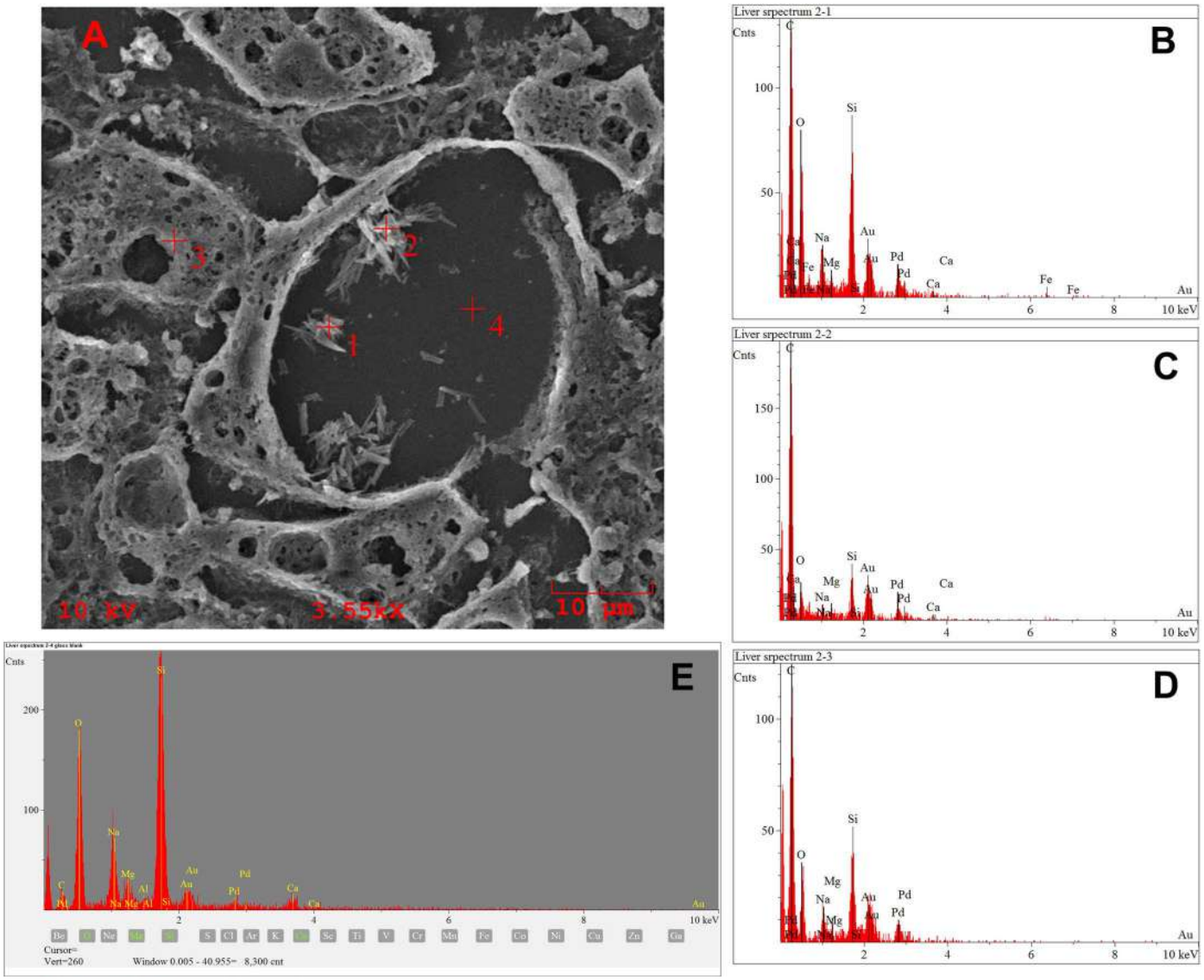

Extended Data Fig. 4 | SEM–EDS imaging of solid inclusions from the hepatic lipid droplets. Locations of EDS are described in the SEM image (**a**). Particles in the droplet (1,2) render carbon-rich spectra (**b**,**c**) compared to a region (3) of hepatic tissue (**d**). The droplet is transected by the sectioning, and thus the background (4) reveals a silica-rich spectra consistent with the glass histology slide (**e**). Importantly, these particulates do not appear to be metallic or mineral. Imaging was conducted on sections from two subjects with consistent findings.

https://doi.org/10.1038/s41591-024-03453-1

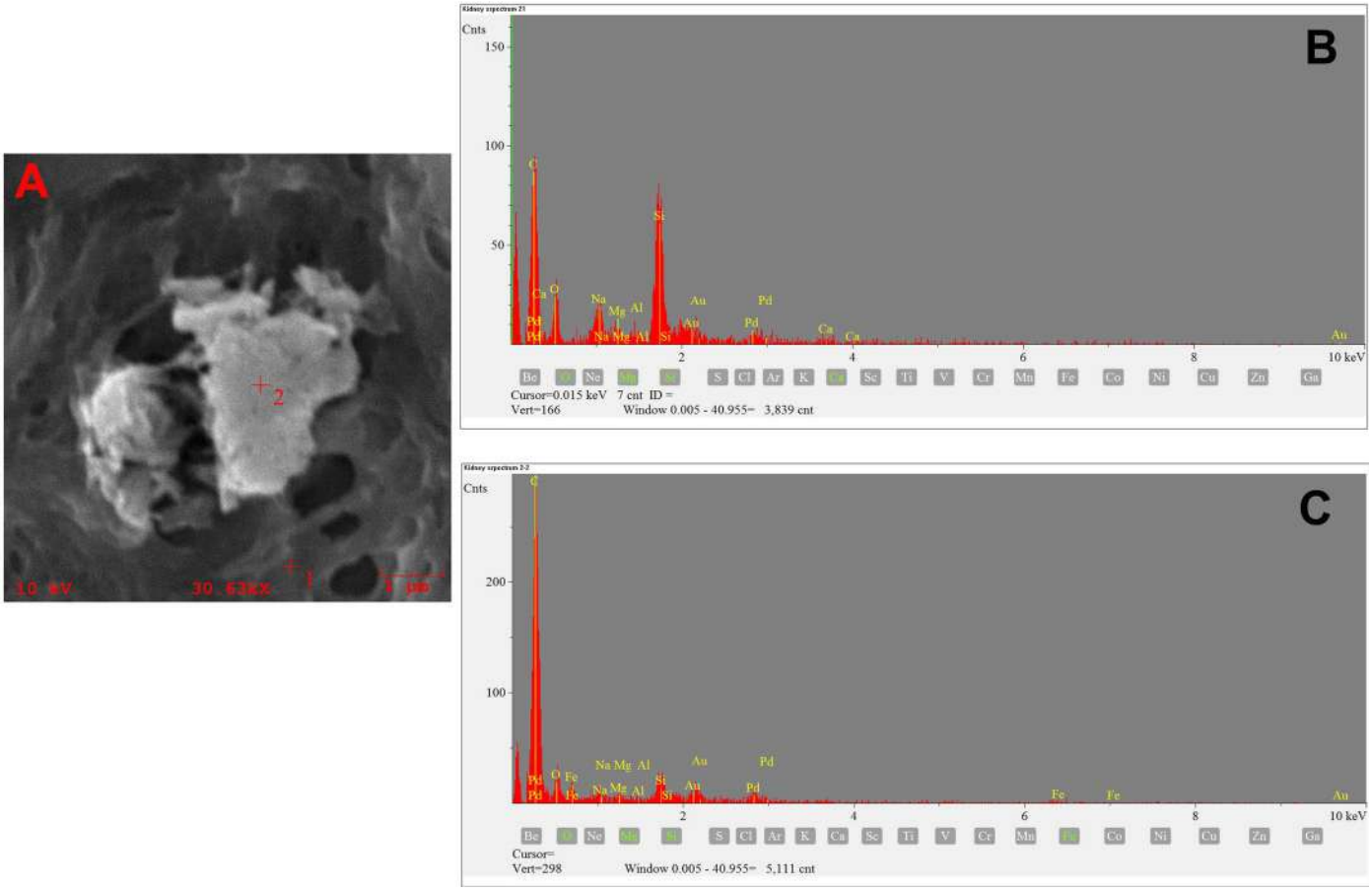

Extended Data Fig. 5 | SEM–EDS imaging of solid inclusions in the kidney. Locations of EDS are described in the SEM image (**a**). Renal tissue (**b**) displays spectra with lower relative carbon concentration than the observed particle (**c**). Importantly, these particulates do not appear to be metallic or mineral. Silicon and gold signals are derived from the mounting media. Imaging was conducted on sections from two subjects with consistent findings.

https://doi.org/10.1038/s41591-024-03453-1

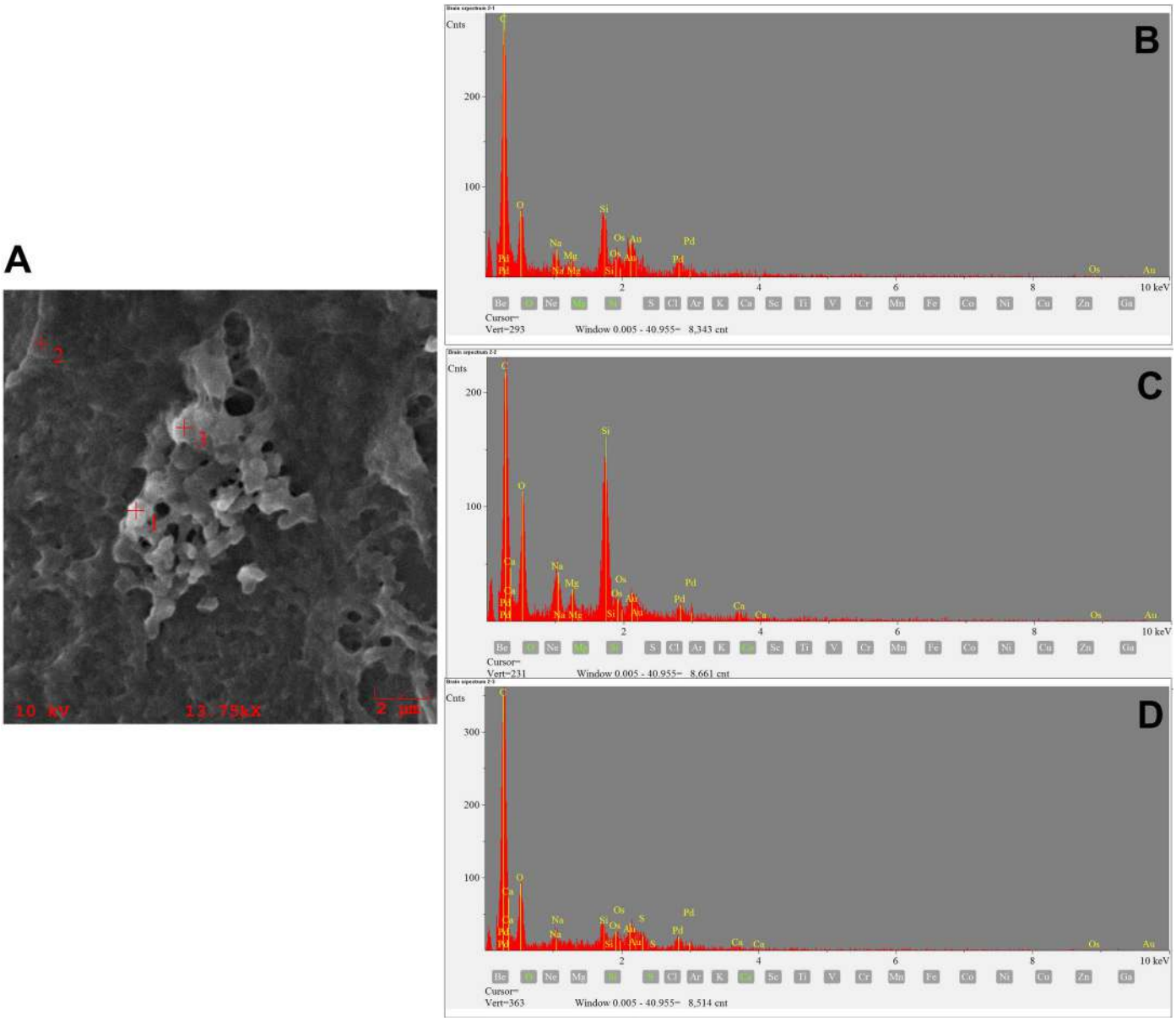

Extended Data Fig. 6 | SEM–EDS imaging of a particulate cluster in a brain specimen. Locations of EDS are described in the SEM image (**a**). The particulate regions (locations 1 and 3) exhibit a greater carbon signal in the spectra (**b**,**d**) compared to the background brain tissue (location 2; **c**). Importantly, these particulates do not appear to be metallic or mineral. Imaging was conducted on sections from two subjects with consistent findings.

https://doi.org/10.1038/s41591-024-03453-1

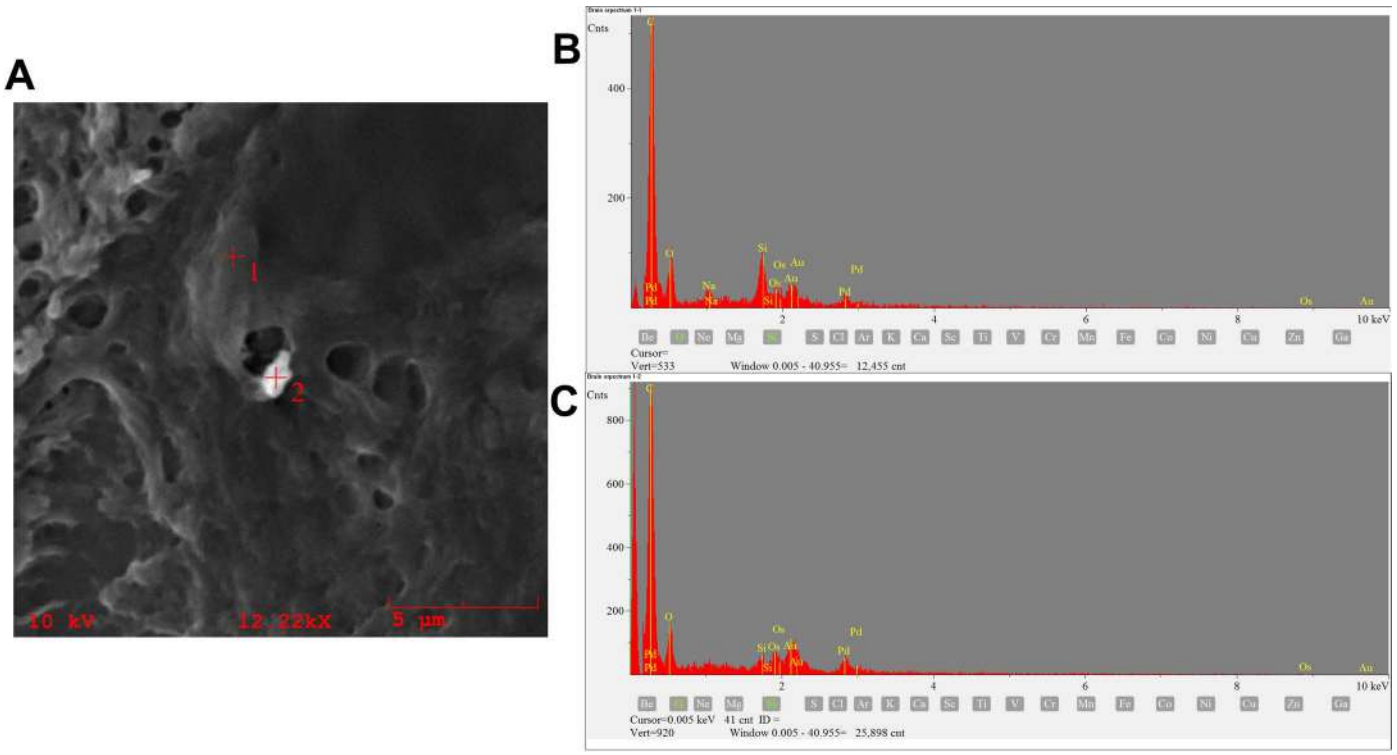

Extended Data Fig. 7 | SEM–EDS imaging of particulate in a brain specimen. Locations of EDS are described in the SEM image (**a**). The background brain tissue (location 1) exhibits a lower carbon signal in the spectrum (**b**) compared to the particulate region (location 2; **c**). Importantly, these particulates do not appear to be metallic or mineral. Imaging was conducted on sections from two subjects with consistent findings.

nature portfolio

Corresponding author(s): Matthew Campen

Last updated by author(s): Dec 5, 2024

Reporting Summary

Nature Portfolio wishes to improve the reproducibility of the work that we publish. This form provides structure for consistency and transparency in reporting. For further information on Nature Portfolio policies, see our Editorial Policies and the Editorial Policy Checklist.

Statistics

For all statistical analyses, confirm that the following items are present in the figure legend, table legend, main text, or Methods section.

n/a	Confirmed
☐	☒ The exact sample size (*n*) for each experimental group/condition, given as a discrete number and unit of measurement
☐	☒ A statement on whether measurements were taken from distinct samples or whether the same sample was measured repeatedly
☐	☒ The statistical test(s) used AND whether they are one- or two-sided *Only common tests should be described solely by name; describe more complex techniques in the Methods section.*
☒	☐ A description of all covariates tested
☐	☒ A description of any assumptions or corrections, such as tests of normality and adjustment for multiple comparisons
☐	☒ A full description of the statistical parameters including central tendency (e.g. means) or other basic estimates (e.g. regression coefficient) AND variation (e.g. standard deviation) or associated estimates of uncertainty (e.g. confidence intervals)
☐	☒ For null hypothesis testing, the test statistic (e.g. *F*, *t*, *r*) with confidence intervals, effect sizes, degrees of freedom and *P* value noted *Give P values as exact values whenever suitable.*
☒	☐ For Bayesian analysis, information on the choice of priors and Markov chain Monte Carlo settings
☒	☐ For hierarchical and complex designs, identification of the appropriate level for tests and full reporting of outcomes
☒	☐ Estimates of effect sizes (e.g. Cohen's *d*, Pearson's *r*), indicating how they were calculated

Our web collection on statistics for biologists contains articles on many of the points above.

Software and code

Policy information about availability of computer code

Data collection	F-Search MPs software v3.7 is a commercial mass spectrometry software from Frontier Labs, Koriyama, Japan.
Data analysis	Statistical analyses were conducted with GraphPad Prism v10.4 (ANOVA, Shapiro-Wilks test, Mann Whitney). Regression analysis was conducted using R version 4.3.3. The MPVAT 2.0 macro was used in ImageJ for FTIR analysis

For manuscripts utilizing custom algorithms or software that are central to the research but not yet described in published literature, software must be made available to editors and reviewers. We strongly encourage code deposition in a community repository (e.g. GitHub). See the Nature Portfolio guidelines for submitting code & software for further information.

Data

Policy information about availability of data

All manuscripts must include a data availability statement. This statement should provide the following information, where applicable:

- Accession codes, unique identifiers, or web links for publicly available datasets
- A description of any restrictions on data availability
- For clinical datasets or third party data, please ensure that the statement adheres to our policy

Data are posted in Dryad. https://doi.org/10.5061/dryad.b8gtht7p8

Human research participants

Policy information about studies involving human research participants and Sex and Gender in Research.

Reporting on sex and gender	Sex was reported for all decedent samples analyzed.
Population characteristics	Limited demographic data (age, sex, race/ethnicity, cause of death, date of death) were available due to the conditions of specimen approval; age of death, race/ethnicity, and sex are reported and considered in regression analyses. The cohort included randomly sampled subjects from the University of New Mexico Office of the Medical Investigator in Albuquerque, New Mexico, along with available samples from the east coast (NC, MD, MA).
Recruitment	Decedent samples were available from the Office of the Medical Investigator.
Ethics oversight	All studies were approved by the UNM Office of the Medical Investigator and UNM Human Research Protections Office, which specifically determined the decedent work to be "not human research".

Note that full information on the approval of the study protocol must also be provided in the manuscript.

Field-specific reporting

Please select the one below that is the best fit for your research. If you are not sure, read the appropriate sections before making your selection.

☒ Life sciences ☐ Behavioural & social sciences ☐ Ecological, evolutionary & environmental sciences

For a reference copy of the document with all sections, see nature.com/documents/nr-reporting-summary-flat.pdf

Life sciences study design

All studies must disclose on these points even when the disclosure is negative.

Sample size	No a priori samples size calculations were performed. Sample sizes were determined largely based on availability and feasibility. This began as an exploratory study with 2016 data and we built the subsequent comparator cohorts based on roughly equal samples sizes. Importantly, with the limited demographic data available, we were able to generate relatively balanced a comparable cohorts in terms of age, sex, and cause of death.
Data exclusions	No data were excluded.
Replication	Samples were prepared and analyzed in such a way that replication was not uniformly feasible due to the consumption of the biospecimens.
Randomization	Samples were procured at random, based on availability from the Office of the Medical Investigator and the collected east coast tissues available from our collaborator (Andrew West). There are no "experimental groups" but the comparisons across date of death trended significantly. We did aim to balance the study across a wide range of ages and causes of death, and collect relatively even male and female samples.
Blinding	Analytical chemistry was conducted without knowledge of decedent characteristics. We were not fully blinded in the sense that subsequent reviewer requests for dementia cases and earlier time frames (ie, "east coast samples") came in batches. Blinding did occur for other demographic data (sex, age, etc).

Reporting for specific materials, systems and methods

We require information from authors about some types of materials, experimental systems and methods used in many studies. Here, indicate whether each material, system or method listed is relevant to your study. If you are not sure if a list item applies to your research, read the appropriate section before selecting a response.

Materials & experimental systems

n/a	Involved in the study
☒	☐ Antibodies
☒	☐ Eukaryotic cell lines
☒	☐ Palaeontology and archaeology
☒	☐ Animals and other organisms
☒	☐ Clinical data
☒	☐ Dual use research of concern

Methods

n/a	Involved in the study
☒	☐ ChIP-seq
☒	☐ Flow cytometry
☒	☐ MRI-based neuroimaging